INTERNATIONAL JOURNAL FOR NUMERICAL METHODS IN FLUIDS
Int. J. Numer. Meth. Fluids 2005; **48**:723–745
Published online 11 March 2005 in Wiley InterScience (www.interscience.wiley.com). DOI: 10.1002/fld.952

Use of slopelimiter techniques in traditional numerical methods for multi-phase flow in pipelines and wells

R. J. Lorentzen*,† and K. K. Fjelde

RF-Rogaland Research, Thormøhlensgt. 55, N-5008 Bergen, Norway

SUMMARY

The aim of this paper is to show how simple and traditional methods for simulating multi-phase flow can be improved by introducing higher order accuracy. Numerical diffusion is reduced to a minimum by using slopelimiter techniques, and better predictions of flow rates and pressure are obtained. Slopelimiter techniques, originally developed to achieve higher order of accuracy in Godunov's method, is applied to a method following a finite element approach and a predictor–corrector shooting technique. These methods are tested and compared to a Godunov-type scheme recently developed for multi-phase flow.

Implementation of Godunov-type schemes for multi-phase flow tends to be a complicated and challenging task. Introducing the slopelimiter techniques in the finite element approach and the predictor–corrector shooting technique is however simple, and provides an overall reduction of the numerical diffusion. The focus is on using these techniques to improve the mass transport description, since this is the main concern in the applications needed.

The presented schemes represent different semi-implicit approaches for simulating multi-phase flow. An evaluation of higher order extensions, as well as a comparison by itself, is of large interest. We present a model for two-phase flow in pipelines and wells, and an outline of the numerical methods and the extensions to second order spatial accuracy. Several examples motivated by applications in underbalanced drilling are presented, and the advantages of using higher order schemes are illustrated.

KEY WORDS: MUSCL technique; implicit methods; two-phase flow

1. INTRODUCTION

Modelling and numerical simulation of two-phase flow in pipelines had its origin in the nuclear energy industry where advanced computer codes like TRAC [1], RELAP [2], and CATHARE [3] were developed for design and safety studies. However, following the development and growth of the petroleum industry, a need evolved for developing dynamic

*Correspondence to: R. J. Lorentzen, RF-Rogaland Research, Thormøhlensgt. 55, N-5008 Bergen, Norway.
†E-mail: rolf.lorentzen@rf.no

Contract/grant sponsor: Norwegian Research Council

Received 26 May 2002
Revised 24 January 2005
Accepted 31 January 2005

computer tools for prediction of multiphase hydrocarbon flow in pipes. On the production side, simulator tools like OLGA [4], PLAC [5] and TACITE [6–10] were developed for design purposes regarding flow of hydrocarbons in production/transport lines. However, in parallel, there has also been developed a class of simulator tools for multi-phase flow occurring during exploration drilling and well interventions. Initially, the main drive here, was the 'kick' scenario which can occur while drilling a well in an overbalanced condition. If a high pressure zone is reached and an uncontrolled gas influx enters the well, immediate reaction is needed by the well crew to initiate certain procedures to bring the gas influx safely out of the system. Examples of simulators developed for these purposes are RF-Kick [11] and SIDEKICK [12, 13]. In the 1990s, the underbalanced drilling technology became more popular. This concept consists of drilling with a mixture of injected gas and liquid. This technique makes it possible to drill with a well pressure substantially lower than the formation pressure, which has a positive effect on both operational time and productivity, see [14]. However, the co-current existence of gas and liquid leads to a highly dynamic system which calls upon improved simulator tools for training and design. Hence, the simulators developed for Kick applications were extended to handle the underbalanced drilling conditions, e.g. RF-Dynaflodrill [15].

Dynamic computer tools for petroleum applications have mainly two objectives: They should give an accurate prediction of downhole pressure and also predict the magnitude of the surface/outlet flow rates. The latter is important for separator design and safety issues and numerical solvers with low numerical diffusion are needed. On the modelling side there have been different approaches. The two fluid model has been used in some models, e.g. OLGA and PLAC, while the simpler drift flux model has been used in models like TACITE, RF-Dynaflodrill and SIDEKICK. The drift flux model use one momentum equation for the mixture opposite to the two fluid model which uses separate momentum equations. Use of the drift flux approach simplifies to some extent the closure problem in the sense that models for the complex interface momentum terms are not needed. However, as the number of equations is reduced by one when adopting the drift flux approach, an additional equation has to be supplied. It is common to include a model for gas slippage, which is an empirical model that describes slippage between phases. In some applications, the drift flux model is simplified further by excluding 'sonic waves'. This is done by removing the acceleration terms in the momentum equation (no pressure wave model). The dynamics in the system are then mainly determined by mass transport and the forces exerted on the system through friction and gravity. This is often sufficient for the applications needed.

In addition to the basic equations, a large number of closure laws (sub models) have to be supplied. This includes complex PVT relations, model for flow pattern description, gas slippage and pressure losses (friction and gravity). Also dynamic modelling of temperature development in the pipeline/well and the surroundings should be included. Development of closure laws is often based on experiments and laboratory work, in addition to more basic modelling.

The governing equations and the closure laws constitute a complex system of first order partial differential equations which calls upon a numerical solution. The models are of hyperbolic nature and include propagation of sound waves and mass (phase volume fraction) waves. The sonic waves are known to have a much faster propagation than the mass waves in the order of ten to thousand in magnitude. Hence, explicit schemes have traditionally been ruled out due to the severe time step restriction induced by the CFL criterion.

The implicit strategies used for solving the models can roughly be broken into three classes. One approach has been direct linearization of the basic equations which then have been solved by a band matrix solver. This approach was used in the first codes developed for the nuclear industry but the OLGA simulator is also using this approach. The numerical methods used were of first order accuracy and gave poor results in terms of numerical diffusion. A remedy for this was to use front tracking of the gas volume waves where e.g. OLGA introduced front tracking of the gas/liquid slugs.

In a different approach used e.g. by RF-Kick and SIDEKICK, the basic equations were solved by a predictor–corrector shooting technique although using different approaches for mass transport. Following this approach, there is no need for direct linearization of the model equations and the closure laws. Numerical diffusion in the RF-Kick simulator has been remedied by local front tracking of the gas volume waves.

Finally, the last approach has been the introduction of Godunov-MUSCL type schemes with the appearance of the TACITE code. These schemes have their origin within the aircraft industry where numerical methods of high accuracy and low numerical diffusion are needed. The accuracy of these schemes rules out the need for local front tracking approaches. However, the original formulation of these schemes requires a detailed mathematical analysis of the underlying model including construction of the appropriate Jacobi matrix and corresponding eigenvalues and eigenvectors. As the basic equations and closure models for multiphase flow in petroleum applications tend to be very complex [8, 9, 16, 17], these constructions have to be done by numerical means leading to larger numerical costs.

In the following, our intention is to present how ideas taken from the Godunov-MUSCL type schemes can be used in more simple numerical approaches used within the gas–oil industry. The MUSCL approach is known to reduce numerical diffusion to a minimum, and more accurate outlet flow rate predictions are obtained. The implementation of these techniques is simple when compared to the use of front tracking techniques. We have applied the MUSCL technique in a predictor–corrector shooting method used in the RF-Kick simulator and also in a newly developed scheme [18] which has some similarities with the OLGA approach.

Finally, two-phase flow modelling involves two kind of errors. Modelling errors caused by ‘inaccuracy’ in the closure laws and numerical errors caused by the way the basic equations are discretized and solved. The first has always had high priority and a lot of work and resources have been spent on developing closure laws as accurate as possible. In this paper, we focus on the latter source of error and potential remedies for this. The model we have chosen is the simple drift flux model, since focus is on numerical aspects. In addition, we also illustrate the difference between using the full drift flux model and the simplified no pressure wave model.

2. DYNAMIC MODEL

A model describing one-dimensional two-phase flow in pipelines consists of nonlinear partial differential equations describing conservation of mass, momentum and energy for each of the phases, see e.g. References [19, 20]. This model is obtained from cross-sectional averaging of the Navier–Stokes equations and viscous stresses are reduced to empirical flow regime dependent terms describing wall and interface friction. In addition, the equations

include complicated terms related to exchanges of mass, momentum and energy through the internal interface or pipe wall. Volume forces due to gravity are essential for the development of vertical flow. This model is known as the two fluid model, and for readers interested in applications we refer to References [4, 5, 10, 21–23]. The two fluid model is used in two main areas. In nuclear reactor plants, focus has been on describing steam/water systems. Examples of model formulations related to this area can be found in References [21–23]. However, the two fluid model has also been used to describe hydrocarbon transport in pipelines in relation to the oil industry. These model formulations are often more complex, due to presence of more complex fluids. In addition the number of conservation laws are higher. In a drilling situation one has to track both drilling fluid, produced oil/gas, produced water, drilled cuttings and also handle the dissolution process of gas versus oil at high pressures/temperatures. In addition, one has to have good models for the slippage between the phases. An example of a more complex two-fluid formulation for petroleum production can be found in Reference [4], but also the formulation presented there is simplified.

The complexity of these models are on of the major reasons why there are so few examples of use of Godunov-type schemes in this area. Since most Godunov-type schemes are based on knowing the eigenstructure of the model it has been difficult to work out proper numerical schemes.

2.1. The drift flux model

The focus of this work is investigation of the accuracy of numerical methods, and we limit ourselves to consider gas–liquid flow in vertical wells. The model we present is quite simplified. For a more general formulation we refer to Reference [8]. We assume that no mass enters or leaves the system through the pipe walls, and we neglect mass transfer between the phases. The simplified mass conservation equations are then written as

$$\frac{\partial}{\partial t}(\alpha_k A \rho_k) + \frac{\partial}{\partial x}(\alpha_k A \rho_k v_k) = 0, \quad k = l, g \tag{1}$$

where l, g represents the liquid and gas phase, respectively, α is the phase, volume fraction, A is the cross-section area, ρ is the density and v is the velocity.

The fundamental two-fluid flow model consists of separate momentum conservation equations for each phase, and includes complicated terms related to phase interaction. It is however a common practice in two-phase modelling to introduce a mixture momentum phase in order to omit modelling of momentum interface terms, see e.g. References [7, 9, 16]. This results in the following equation for the mixture phase (drift flux formulation):

$$\frac{\partial}{\partial t} A(\alpha_l \rho_l v_l + \alpha_g \rho_g v_g) + \frac{\partial}{\partial x} A(\alpha_l \rho_l v_l^2 + \alpha_g \rho_g v_g^2) + A \frac{\partial}{\partial x} p = -Aq \tag{2}$$

where p is pressure and $q = K + \rho_{\text{mix}} g$ represents the external forces acting on the fluids; K represents a friction pressure-loss term and $\rho_{\text{mix}} g$ represents gravitational forces; $\rho_{\text{mix}} = (\rho_g \alpha_g + \rho_l \alpha_l)$ defines the mixture density. We further assume that there is no heat exchange in the fluid, which makes the energy conservation equations redundant (isentropic conditions).

The governing partial differential equations for two-phase flow are insufficient to completely describe the physical processes involved. There are more unknowns than equations and additional closure relations are required. The missing information in the mixture momentum

equation must be replaced by empirical relations which provides information about phase velocities and pressure loss terms. In addition, it is necessary to specify thermodynamic relations, generally derived by assuming a system in thermodynamic equilibrium (PVT models). It is also necessary to provide physical boundary conditions for the system. In this context, the flow rates are assumed to be known at the inlet, and pressure is assumed to be specified at the outlet.

The closure relations usually involve complicated expressions, or they can be given in tabular form based on experimental data. For computational purposes, we use the following simple gas slip relation

$$v_g = C_0 v_{\text{mix}} + C_1 \tag{3}$$

where $v_{\text{mix}} = v_g \alpha_g + v_l \alpha_l$ defines the mixture velocity and C_0 and C_1 are empirical given parameters. The friction pressure loss is modelled by the following simple relation:

$$K = \frac{32 v_{\text{mix}} \mu_{\text{mix}}}{D^2}$$

where D is the inner diameter of the pipe and $\mu_{\text{mix}} = \mu_g \alpha_g + \mu_l \alpha_l$ defines the mixture viscosity. A value of 5×10^{-2} Pa s is adopted for the liquid viscosity, and 5×10^{-6} Pa s for the gas viscosity. The equation relating pressure and density for the gas phase is obtained by assuming an ideal gas law

$$\rho_g = \frac{p}{a_g^2}$$

where $a_g \approx 316$ m/s is the velocity of sound in the gas phase. The liquid density model is given by

$$\rho_l = \rho_0 + \frac{p - p_0}{a_l^2}$$

where constant compressibility is assumed. Here $a_l \approx 1000$ m/s is the velocity of sound in the liquid phase and ρ_0 is the density at a reference pressure p_0.

The drift flux model can also be simplified further by removing the acceleration terms in the momentum equation, see Reference [10]. This model will be referred to as the no pressure wave model. The momentum equation will then be

$$\frac{\partial}{\partial x} p = -K - \rho_{\text{mix}} g \tag{4}$$

This simplification eliminates the sonic waves from the model. As mentioned in Reference [10], most transients of interest in the petroleum industry are related to mass transport effects. If a vertical wall is considered, the pressure distribution is typically dominated by hydrostatic pressures and eventual wall friction effects. Acoustic waves can occur during rate changes or changes in the surface back pressure. However, these waves will only give quite small pressure disturbances which are damped by viscous effects after a short while.

2.2. Characteristics of the model

By assuming a constant cross-sectional flow area, the governing equations for two-phase flow can be written as a system of conservation laws

$$\frac{\partial \mathbf{u}}{\partial t} + \frac{\partial \mathbf{f}}{\partial x} = \mathbf{q} \tag{5}$$

where

$$\mathbf{u} = \begin{pmatrix} \alpha_l \rho_l \\ \alpha_g \rho_g \\ \alpha_l \rho_l v_l + \alpha_g \rho_g v_g \end{pmatrix}, \quad \mathbf{f} = \begin{pmatrix} \alpha_l \rho_l v_l \\ \alpha_g \rho_g v_g \\ \alpha_l \rho_l v_l^2 + \alpha_g \rho_g v_g^2 + p \end{pmatrix}, \quad \mathbf{q} = \begin{pmatrix} 0 \\ 0 \\ -q \end{pmatrix}$$

These equations can also be expressed in quasi-linear form

$$\frac{\partial \mathbf{u}}{\partial t} + \mathbf{A}(\mathbf{u}) \frac{\partial \mathbf{u}}{\partial x} = \mathbf{q} \tag{6}$$

where $\mathbf{A}(\mathbf{u})$ is the Jacobi matrix of the flux function versus the conservative variables. Some details regarding the flux functions are included in Appendix. This system of conservation laws has been analysed by Théron [24] and Gavage [25]. The model was shown to be hyperbolic in a physically reasonable region of parameters and three distinct and real eigenvalues were obtained. Two of the eigenvalues (λ_1 and λ_3) correspond to rapid sonic waves (pressure pulses) propagating in the upstream and downstream direction of the fluid flow, while the last eigenvalue (λ_2) is associated to mass (phase volume fraction) waves. Gavage showed that the approximate eigenvalues of the system was $\lambda_1 = v_l - w$, $\lambda_2 = v_g$ and $\lambda_3 = v_l + w$, where the sound velocity was approximated by:

$$w = \sqrt{\frac{p}{\alpha_g \rho_l (1 - C_0 \alpha_g)}}$$

She had to assume a constant liquid density and perform some linearization to obtain these approximate algebraic expressions. Hence, obtaining algebraic expressions for a more complex drift flux model seems out of range, and numerical methods based on knowing eigenvalues/eigenstructures must use numerical approximations for obtaining these. The eigenvalues corresponding to the pressure pulses are generally 10-100 times larger than the eigenvalue corresponding to the mass transport, i.e. $|\lambda_1|, |\lambda_3| \gg |\lambda_2|$. Eigenvalues are essential in Godunov-type schemes, and will be discussed further in Section 3.3.

3. NUMERICAL METHODS

The non-linear and coupled characteristic of the drift-flux model makes it impossible to solve the equations analytically, and a numerical solution strategy is required. The aim of a numerical solver is to compute accurate and stable approximations of the flow variables (e.g. pressure, velocity, volume fractions, etc.). Numerical methods replace the continuous problem represented by Equations (1) and (2) by a finite set of discrete values. These values are defined on a mesh composed of cells in the (x, t) plane. The pipe section of length $[0, L]$

is divided into M segments $[x_{i-1/2}, x_{i+1/2}]$, where $x_{1/2} = 0$ and $x_{M+1/2} = L$. We let x_i denote the centres of the segments, and the time levels are denoted t_n. The spacing in the x and t variables is denoted Δx and Δt.

A numerical method is explicit if the discretized flow variables at the previous time level (t_n) are used to calculate the flow variables at the new time level (t_{n+1}). The time step is limited by the CFL condition

$$\Delta t \leqslant \frac{\Delta x}{\max(\lambda_1, \lambda_2, \lambda_3)}$$

In many drilling situations, such as gas-kick scenarios and underbalanced drilling operations, the dynamic behavior lasts in order of hours. The CFL condition will therefore imply large computational time if explicit methods are used to simulate these situations.

Fully implicit methods are not limited by the CFL condition, but they have the disadvantage of smearing out discontinuities. The methods described in this section are semi-implicit in the sense that pressure calculations are based on implicit solution techniques, and the mass transport is treated explicit. The time step is thus limited by a CFL condition depending on the mass transport signal ($\Delta x/\lambda_2$). Some of the solution details are thus sacrificed to increase computational efficiency.

The rest of this chapter is organized as follows: First, a numerical method based on a finite element approach is presented. This method results in an integration of the momentum equation along characteristics. The second method is a predictor–corrector shooting technique, and the last method is a semi-implicit version of the conservative Roe-scheme, see References [9, 26, 27]. The extension to second order spatial accuracy is discussed at the end of the chapter.

3.1. A finite element approach

In this section the solution strategy for a recently developed semi-implicit method [18] is presented. The solution process requires a rearrangement of the governing equations, which involve introduction of total mass flux $F = A(\alpha_l \rho_l v_l + \alpha_g \rho_g v_g)$, and centre of mass velocity $v_{\text{com}} = F/A\rho_{\text{mix}}$. To simplify future calculations, we also redefine the friction factor by the relation $K \to \tilde{K}F$. By adding the mass conservation equations, we obtain the following equation for conservation of total mass:

$$A\kappa \frac{\partial p}{\partial t} + \frac{\partial F}{\partial x} = 0 \tag{7}$$

where $\kappa = \partial \rho_{\text{mix}}/\partial p$. Following the outline in Reference [18], the momentum equation (2) is simplified as

$$\frac{\partial F}{\partial t} + \frac{\partial v_{\text{com}} F}{\partial x} + A\frac{\partial p}{\partial x} + \tilde{K}F = -A\rho_{\text{mix}} g \tag{8}$$

Here, terms involving $(v_l - v_g)$ is neglected.

To proceed, we define a test function β_i which is constant over segment i, and zero elsewhere. We then integrate Equation (7) with the test function β_i over the space and time strip

$\Omega = [0, L] \times [t_n, t_{n+1}]$. Integration by parts yields

$$\int_0^L [A\beta_i \kappa p]_{t_n}^{t_{n+1}} \, \mathrm{d}x - \int_\Omega pA\kappa \frac{\partial \beta_i}{\partial t} \, \mathrm{d}\Omega + \int_{t_n}^{t_{n+1}} [\beta_i F]_0^L \, \mathrm{d}t - \int_\Omega F \frac{\partial \beta_i}{\partial x} \, \mathrm{d}\Omega = 0$$

which is reduced to an equation of the form

$$v_i^a p_i^{n+1} + v_i^b (F_{i+1/2}^{n+1} - F_{i-1/2}^{n+1}) = v_i^c \tag{9}$$

where v_i^a, v_i^b and v_i^c are coefficients given from the integration.

We then multiply Equation (8) with a space–time test function β. Integration by parts over Ω yields

$$\int_0^L [F\beta]_{t_n}^{t_{n+1}} \, \mathrm{d}x + \int_{t_n}^{t_{n+1}} [v_{\mathrm{com}} F\beta]_0^L \, \mathrm{d}t - \int_\Omega F(\beta_t + v_{\mathrm{com}} \beta_x - \beta \tilde{K}) \, \mathrm{d}\Omega$$
$$+ \int_\Omega A \frac{\partial p}{\partial x} \beta \, \mathrm{d}\Omega = - \int_\Omega A \rho_{\mathrm{mix}} g \beta \, \mathrm{d}\Omega \tag{10}$$

We then take the test function β to fulfill the adjoint equation

$$\beta_t + v_{\mathrm{com}} \beta_x = 0$$

which gives a test function on the form

$$\beta(x, t) = \beta(x - v_{\mathrm{com}}(t - t_{n+1}))$$

We then define the following left and right basis functions

$$\beta_L(x, t) = \frac{1}{\Delta x}[(x_{i+1/2} - x) + v_{\mathrm{com}}(t - t_{n+1})]$$

and

$$\beta_R(x, t) = \frac{1}{\Delta x}[(x - x_{i-1/2}) - v_{\mathrm{com}}(t - t_{n+1})]$$

where $x_{i-1/2} + v_{\mathrm{com}}(t - t_{n+1}) < x < x_{i+1/2} + v_{\mathrm{com}}(t - t_{n+1})$ and $t_n < t < t_{n+1}$. The centre of mass velocity is evaluated at the cell boundaries at time t_n. We evaluate (10) by applying β equal to the left and right basis function respectively on the domain specified above, and zero elsewhere. The following two equations are then obtained:

$$\xi_{iL}^a F_{i-1/2}^{n+1} + \xi_{iL}^b p_{i-1/2}^{n+1} + \xi_{iL}^c p_i^{n+1} = \xi_{iL}^d \tag{11}$$

$$\xi_{iR}^a F_{i+1/2}^{n+1} + \xi_{iR}^b p_{i+1/2}^{n+1} + \xi_{iR}^c p_i^{n+1} = \xi_{iR}^d \tag{12}$$

where $p_{i-1/2}^{n+1}$ and $p_{i+1/2}^{n+1}$ are pressures evaluated at the left and right boundary, respectively. The coefficients in Equations (11) and (12) follow from integration of (10).

We can now eliminate p_i^{n+1} from Equations (11) and (12) by using Equation (9). The following equations are then obtained:

$$\tilde{\xi}_{iL}^a F_{i-1/2}^{n+1} + \xi_{iL}^b p_{i-1/2}^{n+1} + \tilde{\xi}_{iL}^c F_{i+1/2}^{n+1} = \tilde{\xi}_{iL}^d \tag{13}$$

and

$$\tilde{\zeta}^a_{iR} F^{n+1}_{i-1/2} + \zeta^b_{iR} p^{n+1}_{i+1/2} + \tilde{\zeta}^c_{iR} F^{n+1}_{i+1/2} = \tilde{\zeta}^d_{iR} \tag{14}$$

Using Equations (13) and (14), $F^{n+1}_{i-1/2}$ and $F^{n+1}_{i+1/2}$ can be expressed in terms of $p^{n+1}_{i-1/2}$ and $p^{n+1}_{i+1/2}$

$$F^{n+1}_{i-1/2} = \eta^a_{iL} p^{n+1}_{i-1/2} + \eta^b_{iL} p^n_{i+1/2} + \eta^c_{iL} \tag{15}$$

$$F^{n+1}_{i+1/2} = \eta^a_{iR} p^{n+1}_{i-1/2} + \eta^b_{iR} p^n_{i+1/2} + \eta^c_{iR} \tag{16}$$

We assume that the flux and pressure are continuous at the cell boundaries which gives the following linear system

$$a_{j,0} p^{n+1}_{j-1/2} + a_{j,1} p^{n+1}_{j+1/2} + a_{j,2} p^{n+1}_{j+3/2} = b_j, \quad j = 1, \ldots, M-1 \tag{17}$$

This system, together with the physical boundary conditions, forms a tridiagonal matrix which is solved using direct substitution. The coefficients in Equations (13)–(17) are functions of the coefficients in Equation (9) and Equations (11)–(12). When the pressure values are known, the left and right fluxes are calculated by using Equations (15) and (16). Equation (9) is then used to calculate the average cell pressure p^{n+1}_i.

The next task is to update the mass distribution, based on pressure and flux at the new time level. This procedure starts at the inlet, where mass rates are given by the physical boundary conditions. The mass distribution is then updated sequentially until the outlet is reached:

1. Temporary velocities $v^*_{k,i+1/2}$, $k = l, g$, are calculated by utilizing Equation (3), the downstream flux $F^{n+1}_{i+1/2}$, and the old volume fraction.
2. The mass in each cell ($M_{k,i}$) is updated for each phase according to

$$M^{n+1}_{k,i} = M^n_{k,i} + \Delta t f^{n+1}_{k,i-1/2} - \Delta t f^{n+1}_{k,i+1/2}, \quad k = l, g$$

   where the downstream flux for each phase ($f_{k,i+1/2}$) is composed by using the intermediate velocity and the upstream volume fraction and density.
3. The new masses are used to calculate final volume fractions $\alpha^{n+1}_{k,i}$, $k = l, g$. Step 1 is then repeated, and final velocities are determined.

3.2. A predictor–corrector shooting technique

A predictor–corrector approach makes it possible to solve Equations (1) and (2) without direct linearization of the governing equations and the closure relations. The method described in this section was originally developed to handle gas-kick situations [11], but can also be used for general dynamic two-phase flow simulations. We give a brief description of the solution strategy.

The no pressure wave model is applied here, i.e. the acceleration terms related to the sonic waves are neglected from the momentum equation:

$$\frac{\partial}{\partial x} p = -q \tag{18}$$

The errors introduced by this approximation are discussed in Section 4.3. The solution algorithm is initiated by making a guess for the inlet pressure. Mass rates at the inlet are given

by the physical boundary conditions. A predictor–corrector algorithm is then used to solve Equations (18) and the mass conservation equations (1), which determines the downstream flow variables in the first cell (see the description below). This also determines the upstream variables for the next cell, by imposing continuity of pressure and mass rates over the cell boundary. This procedure is sequentially repeated for each cell until the outlet is reached. The calculated outlet pressure is then compared to the pressure given by the physical boundary condition. The inlet pressure is iterated until the calculated outlet pressure has converged. It should be mentioned that a similar approach was pursued by Nickens [12], although he did not neglect the pressure pulses.

We now give a short description of the predictor and corrector steps in the algorithm. The predictor step starts by using a discretized version of Equation (18) to calculate a temporary downstream pressure at the new time level in cell i (based on old variables):

$$p^*_{i+1/2} = p^{n+1}_{i-1/2} - \Delta x q^n_i \tag{19}$$

The known upstream pressure is either given by the updated solution in the upstream cell, or by the guess made for the inlet pressure. The average cell pressure is then given by

$$p^*_i = \frac{p^*_{i+1/2} + p^{n+1}_{i-1/2}}{2} \tag{20}$$

The updated pressure is then used to calculate the mass distribution. To proceed, a guess is made for the downstream mixture velocity, $v^*_{\mathrm{mix},i+1/2}$, and the temporary mass in cell i is calculated by

$$M^*_{k,i} = M^n_{k,i} + \Delta t f^{n+1}_{k,i-1/2} - \Delta t f^*_{k,i+1/2}, \quad k = l, g \tag{21}$$

where the downstream flux is a function of $v^*_{\mathrm{mix},i+1/2}$. The following volume balance equation is then solved by iteration, which determines the downstream mixture velocity:

$$g(v^*_{\mathrm{mix},i+1/2}) \equiv V^*_i(v^*_{\mathrm{mix},i+1/2}) - A\Delta x = 0 \tag{22}$$

where

$$V^*_i(v^*_{\mathrm{mix},i+1/2}) = \frac{M^*_{l,i}}{\rho_l(p^*)} + \frac{M^*_{g,i}}{\rho_g(p^*)}$$

The corrector step consists of repeating the steps (19)–(22) using updated flow variables. This procedure is continued until the flow variables in the cell have converged. The variables $p^{n+1}_{i+1/2}$, p^{n+1}_i, $v^{n+1}_{\mathrm{mix},i+1/2}$, $M^{n+1}_{l,i}$ and $M^{n+1}_{g,i}$ are then determined.

3.3. A Godunov-type scheme

The numerical approach described in this section departs from the schemes outlined in the previous sections, as the system of conservation laws (5) is solved in a fully coupled manner. A conservative explicit finite volume scheme for Equation (5) has the form

$$\mathbf{U}^{n+1}_i = \mathbf{U}^n_i - \frac{\Delta t}{\Delta x}(\mathbf{F}^n_{i+1/2} - \mathbf{F}^n_{i-1/2}) + \Delta t \mathbf{Q}^n_i \tag{23}$$

where $\mathbf{F}^n_{i+1/2}$ is an approximation of the flux $\mathbf{f}(\mathbf{u}(x,t))$ at $x_{i+1/2}$, and $\mathbf{Q}^n_i = \mathbf{q}(\mathbf{U}^n_i)$. For an introduction to numerical schemes for conservation laws, see e.g. References [28–30]. We

propose a scheme based on a semi-implicit approach described by Faille *et al.* [9], and the numerical Roe scheme, see References [26, 27]. The traditional Godunov scheme involves the exact solution of a large number of Riemann problems, and is a complicated and time consuming process. Simplification of this method was therefore introduced by the development of *approximate Riemann solvers*. Roe's approximate Riemann solver is based on the solution of the linearized Riemann problem

$$\frac{\partial \mathbf{u}}{\partial t} + \hat{\mathbf{A}}(\mathbf{U}_i^n, \mathbf{U}_{i+1}^n)\frac{\partial \mathbf{u}}{\partial x} = 0, \quad \mathbf{u}(x,0) = \begin{cases} \mathbf{U}_i^n & \text{for } x \leqslant x_{i+1/2} \\ \mathbf{U}_{i+1}^n & \text{for } x > x_{i+1/2} \end{cases} \tag{24}$$

where the matrix $\hat{\mathbf{A}}(\mathbf{U}_i^n, \mathbf{U}_{i+1}^n)$ is an approximation of the Jacobi matrix, and must satisfy the following conditions:

(i) $\hat{\mathbf{A}}(\mathbf{U}_i^n, \mathbf{U}_{i+1}^n)$ has only real eigenvalues and is diagonalizable.
(ii) $\mathbf{f}(\mathbf{U}_{i+1}^n) - \mathbf{f}(\mathbf{U}_i^n) = \hat{\mathbf{A}}(\mathbf{U}_i^n, \mathbf{U}_{i+1}^n)(\mathbf{U}_{i+1}^n - \mathbf{U}_i^n)$.
(iii) $\hat{\mathbf{A}}(\mathbf{U}_i^n, \mathbf{U}_{i+1}^n) \to \mathbf{A}(\mathbf{u})$ as $\mathbf{U}_{i+1}^n, \mathbf{U}_i^n \to \mathbf{u}$.

Condition (i) ensures hyperbolicity, condition (ii) is needed to achieve conservation across discontinuities and condition (iii) ensures consistency with the exact Jacobian. The numerical flux for the Roe scheme is then given by

$$\mathbf{F}_{i+1/2}^n = \tfrac{1}{2}(\mathbf{f}(\mathbf{U}_i^n) + \mathbf{f}(\mathbf{U}_{i+1}^n)) - \tfrac{1}{2}|\hat{\mathbf{A}}_{i+1/2}^n|(\mathbf{U}_{i+1}^n - \mathbf{U}_i^n) \tag{25}$$

where $\hat{\mathbf{A}}_{i+1/2}^n = \hat{\mathbf{A}}(\mathbf{U}_i^n, \mathbf{U}_{i+1}^n)$ and $|\hat{\mathbf{A}}_{i+1/2}^n|$ is the matrix which has the same eigenvectors as $\hat{\mathbf{A}}_{i+1/2}^n$, and eigenvalues equal to the absolute values of the eigenvalues of $\hat{\mathbf{A}}_{i+1/2}^n$. In order to construct a Roe matrix $\hat{\mathbf{A}}$, we first define the Jacobian $\bar{\mathbf{A}} \equiv \mathbf{A}(\mathbf{U}_{i+1/2}^n)$, where $\mathbf{U}_{i+1/2}^n = \frac{1}{2}(\mathbf{U}_i^n + \mathbf{U}_{i+1}^n)$. This matrix satisfies (i) and (iii). In order to make it satisfy (ii), we follow the approach described in References [16, 27]. We first decompose the Jacobian $\bar{\mathbf{A}}$ as $\bar{\mathbf{A}} = \bar{\mathbf{R}}\bar{\mathbf{\Lambda}}\bar{\mathbf{R}}^{-1}$, where $\bar{\mathbf{R}}$ is the right eigenvector matrix, and $\bar{\mathbf{\Lambda}}$ is the matrix having the eigenvalues of $\bar{\mathbf{A}}$ at its diagonal. Next, we determine a diagonal matrix $\hat{\mathbf{\Lambda}}$ such that $\bar{\mathbf{R}}\hat{\mathbf{\Lambda}}\bar{\mathbf{R}}^{-1}\Delta\mathbf{U} = \Delta\mathbf{f}$, where $\Delta\mathbf{U} = \mathbf{U}_{i+1}^n - \mathbf{U}_i^n$ and $\Delta\mathbf{f} = \mathbf{f}(\mathbf{U}_{i+1}^n) - \mathbf{f}(\mathbf{U}_i^n)$. The Roe matrix $\hat{\mathbf{A}}$ is then defined by

$$\hat{\mathbf{A}} = \hat{\mathbf{A}}(\mathbf{U}_i^n, \mathbf{U}_{i+1}^n) = \begin{cases} \bar{\mathbf{R}}\hat{\mathbf{\Lambda}}\bar{\mathbf{R}}^{-1} & \text{if } \mathbf{U}_i^n \neq \mathbf{U}_{i+1}^n \\ \bar{\mathbf{R}}\bar{\mathbf{\Lambda}}\bar{\mathbf{R}}^{-1} & \text{if } \mathbf{U}_i^n = \mathbf{U}_{i+1}^n \end{cases} \tag{26}$$

An implicit version of the numerical scheme (23) is obtained (see Reference [9]) by evaluating the numerical flux given by Equation (25) at the new time level: $\mathbf{F}_{i+1/2}^{n+1} = \mathbf{F}(\mathbf{U}_i^{n+1}, \mathbf{U}_{i+1}^{n+1})$. We also evaluate the source term at the new time level: $\mathbf{Q}_i^{n+1} = \mathbf{Q}(\mathbf{U}_i^{n+1})$. These expressions are then linearized by using a first order Taylor expansion with respect to $\mathbf{U}_i^n$ and $\mathbf{U}_{i+1}^n$:

$$\mathbf{F}(\mathbf{U}_i^{n+1}, \mathbf{U}_{i+1}^{n+1}) \approx \mathbf{F}(\mathbf{U}_i^n, \mathbf{U}_{i+1}^n) + \frac{\partial \mathbf{F}(\mathbf{U}_i^n, \mathbf{U}_{i+1}^n)}{\partial \mathbf{U}_i^n}(\mathbf{U}_i^{n+1} - \mathbf{U}_i^n) + \frac{\partial \mathbf{F}(\mathbf{U}_i^n, \mathbf{U}_{i+1}^n)}{\partial \mathbf{U}_{i+1}^n}(\mathbf{U}_{i+1}^{n+1} - \mathbf{U}_{i+1}^n) \tag{27}$$

$$\mathbf{Q}(\mathbf{U}_i^{n+1}) \approx \mathbf{Q}(\mathbf{U}_i^n) + \frac{\partial \mathbf{Q}(\mathbf{U}_i^n)}{\partial \mathbf{U}_i^n}(\mathbf{U}_i^{n+1} - \mathbf{U}_i^n) \tag{28}$$

By assuming that $|\hat{\mathbf{A}}_{i+1/2}^n|$ is constant, the expressions in Equation (27) becomes

$$\frac{\partial \mathbf{F}(\mathbf{U}_i^n, \mathbf{U}_{i+1}^n)}{\partial \mathbf{U}_i^n} \approx \frac{1}{2}(\mathbf{A}_i^n + |\hat{\mathbf{A}}_{i+1/2}^n|) \tag{29}$$

$$\frac{\partial \mathbf{F}(\mathbf{U}_i^n, \mathbf{U}_{i+1}^n)}{\partial \mathbf{U}_{i+1}^n} \approx \frac{1}{2}(\mathbf{A}_{i+1}^n - |\hat{\mathbf{A}}_{i+1/2}^n|) \tag{30}$$

where $\mathbf{A}_i^n = \mathbf{A}(\mathbf{U}_i^n)$.

Faille *et al.* [9] proposed a way to modify this scheme in order to keep the accuracy on the slow wave (λ_2), while maintaining implicit treatment of the fast waves (λ_1 and λ_3). Equations (29) and (30) are replaced by

$$\frac{\partial \mathbf{F}(\mathbf{U}_i^n, \mathbf{U}_{i+1}^n)}{\partial \mathbf{U}_i^n} \approx \frac{1}{2}(\tilde{\mathbf{A}}_i^n + |\tilde{\hat{\mathbf{A}}}_{i+1/2}^n|) \tag{31}$$

$$\frac{\partial \mathbf{F}(\mathbf{U}_i^n, \mathbf{U}_{i+1}^n)}{\partial \mathbf{U}_{i+1}^n} \approx \frac{1}{2}(\tilde{\mathbf{A}}_{i+1}^n - |\tilde{\hat{\mathbf{A}}}_{i+1/2}^n|) \tag{32}$$

where $\tilde{\mathbf{A}}$ has the same eigenvectors as $\mathbf{A}$, but the eigenvalues are replaced by $\tilde{\lambda}_1 = \lambda_1$, $\tilde{\lambda}_2 = 0$ and $\tilde{\lambda}_3 = \lambda_3$. The matrix $\tilde{\hat{\mathbf{A}}}$ is obtained in the same manner. The scheme is then divided into two stages

1. An explicit step

$$\delta \mathbf{U}_i^* = -\frac{\Delta t}{\Delta x}(\mathbf{F}(\mathbf{U}_i^n, \mathbf{U}_{i+1}^n) - \mathbf{F}(\mathbf{U}_{i-1}^n, \mathbf{U}_i^n)) + \Delta t \mathbf{Q}_i^n$$

2. An implicit step which will stabilize the explicit solution

$$-\frac{\Delta t}{2\Delta x}[\tilde{\mathbf{A}}_{i-1}^n + |\tilde{\hat{\mathbf{A}}}_{i-1/2}^n|]\delta \mathbf{U}_{i-1} + \left[\mathbf{I} + \frac{\Delta t}{2\Delta x}(|\tilde{\hat{\mathbf{A}}}_{i+1/2}^n| + |\tilde{\hat{\mathbf{A}}}_{i-1/2}^n|) - \Delta t \mathbf{D}\mathbf{Q}_i^n\right]\delta \mathbf{U}_i$$
$$+\frac{\Delta t}{2\Delta x}[\tilde{\mathbf{A}}_{i+1}^n - |\tilde{\hat{\mathbf{A}}}_{i+1/2}^n|]\delta \mathbf{U}_{i-1} = \delta \mathbf{U}_i^*$$

where $\delta \mathbf{U}_i = \mathbf{U}_i^{n+1} - \mathbf{U}_i^n$, $\mathbf{I}$ is the identity matrix and $\mathbf{D}\mathbf{Q}_i^n = \partial \mathbf{Q}(\mathbf{U}_i^n)/\partial \mathbf{U}_i^n$.

The application of the numerical scheme at the boundary cells $i = 1$ and M, requires the numerical flux values $\mathbf{F}_{1/2}$ and $\mathbf{F}_{M+1/2}$. These fluxes cannot be calculated directly, as $\mathbf{U}_0$ and $\mathbf{U}_{M+1}$ are outside the computational domain. The information which is not given by the physical boundary conditions must be supplied by additional information. We have used a *ghost*

cell technique, which is based on defining external cells (ghost cells) outside the computational domain. The values in these cells are calculated by combining the physical boundary conditions, and information obtained from the wave structure of the Riemann problems at the boundaries, see Reference [31].

3.4. Second order schemes

The high amount of numerical diffusion in first order schemes makes it impossible to reconstruct sharp fronts accurately. It is on the other hand well known that classical higher order linear schemes produce spurious oscillations in the vicinity of large gradients. This has lead to the introduction of *total variation diminishing* (TVD) schemes. TVD schemes are of high order, and have the property of non-increasing total variation. Unphysical oscillations are thus avoided. The methods were originally developed for scalar one-dimensional problems, but a large number of successful applications to systems of conservations laws exist [28, 30]. In this paper we use a slopelimiter, or MUSCL (abbreviation for *Monotone Upstream-centred Scheme for Conservation Laws*) technique, which fulfills the TVD condition. The MUSCL/slopelimiter method was first introduced by van Leer [32, 33], and is based on a piece-wise linear reconstruction of the cell averages.

We have chosen to represent the cell averages in terms of the primitive variables $\mathbf{p}=(p,\alpha_g,v_l)$. A linear reconstruction is then given by

$$\mathbf{P}_i(x)=\mathbf{P}_i+(x-x_i)\boldsymbol{\Delta}_i,\quad x\in[x_{i-1/2},x_{i+1/2}] \tag{33}$$

where $\boldsymbol{\Delta}_i$ denotes a suitable (limited) slope constructed from the cell averages $\mathbf{P}_i$.

There exists a variety of limiters which can be used to calculate the slopes $\boldsymbol{\Delta}_i$. MINMOD is the most diffusive limiter, while SUPERBEE is known to be over-compressive. We use the smooth VANLEER limiter, which lies between MINMOD and SUPERBEE. For further details on TVD methods and MUSCL/slopelimiter type high order methods, we refer to References [28–30].

The numerical methods described in Sections 3.1–3.3 use the extrapolated primitive variables at the cell boundaries for evaluation of the fluxes. The extrapolated variables are given by

$$\mathbf{P}_{i-1/2,+}=\mathbf{P}_i^n-\frac{\Delta x}{2}\boldsymbol{\Delta}_i,\quad \mathbf{P}_{i+1/2,-}=\mathbf{P}_i^n+\frac{\Delta x}{2}\boldsymbol{\Delta}_i$$

see Figure 1.

The finite element approach and the predictor–corrector shooting technique use the extrapolated values for pressure and volume fraction ($\alpha_{i-1/2,+}$, $\alpha_{i+1/2,-}$, $p_{i-1/2,+}$, $p_{i+1/2,-}$) to evaluate the mass transport fluxes. The velocity at the boundaries is found by iteration of the mass conservation equations. The Godunov-type scheme is extended to second order by using the extreme values $\mathbf{U}_{i+1/2,+}$ and $\mathbf{U}_{i+1/2,-}$ in the numerical flux:

$$\mathbf{F}_{i+1/2}=\tfrac{1}{2}(\mathbf{f}(\mathbf{U}_{i+1/2,-})+\mathbf{f}(\mathbf{U}_{i+1/2,+}))-\tfrac{1}{2}|\hat{\mathbf{A}}_{i+1/2}|(\mathbf{U}_{i+1/2,+}-\mathbf{U}_{i+1/2,-}) \tag{34}$$

where $\hat{\mathbf{A}}_{i+1/2}=\hat{\mathbf{A}}(\mathbf{U}_{i+1/2,-},\mathbf{U}_{i+1/2,+})$. The extreme values $\mathbf{U}_{i+1/2,+}$ and $\mathbf{U}_{i+1/2,-}$ are calculated by converting the extrapolated primitive variables.

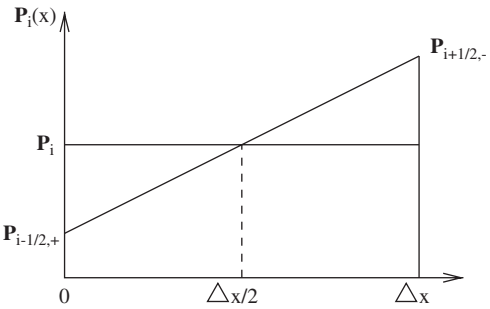

Figure 1. Piece-wise linear reconstruction of the primitive variables in cell i.

4. NUMERICAL RESULTS

The examples in this section are motivated by dynamical effects present in underbalanced drilling operations. We have chosen test scenarios where gas and liquid are injected at the bottom of the well. Gas is injected in order to obtain reduced hydrostatic pressure, leading to an underbalanced condition. The main variables of interest in such operations are the bottom hole pressure and the outlet flow rates. Control of the bottom hole pressure is important in order to maintain the underbalanced condition, and the prediction of the outlet flow rates is crucial for proper separator design. We wish to illustrate how numerical diffusion affects prediction of these variables and show the advantage of using second order schemes. The well configuration consists of a 1000 m deep vertical well with a 0.1 m inner diameter. The outlet pressure is kept constant equal to 6 bar. The grid length is 20 m and the time step is 1 s. In the following, the finite element approach is abbreviated FE, and the predictor–corrector shooting technique is abbreviated PCS. We have chosen to use the second order Godunov type scheme as a reference case. This scheme is then compared with the first and second order versions of the predictor corrector shooting technique and the finite element approach. One should expect that the first order version of all the schemes will basically give the same results, since all of them will typically be first order upwind schemes in this case. Hence, we have not included results for the 1st order Godunov scheme. The intention of the comparison is to show that the first order versions of the simpler predictor scheme and FE approach have problems with numerical diffusion when comparing with the more accurate results obtained by the second order Godunov scheme. However, we see that more accurate results can be obtained by using the slope limit approach in these simpler/traditional schemes. The second order versions of these schemes give results that are quite comparable with the second order Godunov scheme.

4.1. Example 1

We consider a well which is initially filled with stagnant liquid. Gas and liquid are then injected at the bottom of the well. The flow rates are increased to 7.5 kg/s for liquid and 0.05kg/s for gas during a 10s period. For simplicity, a no-slip condition is used, i.e. $C_0 = 1$ and $C_1 = 0$ in Equation (3). The no-slip condition is physical reasonable when the dispersed bubble flow pattern is present. Figures 2–4 show the bottom hole pressure and the outlet flow rates

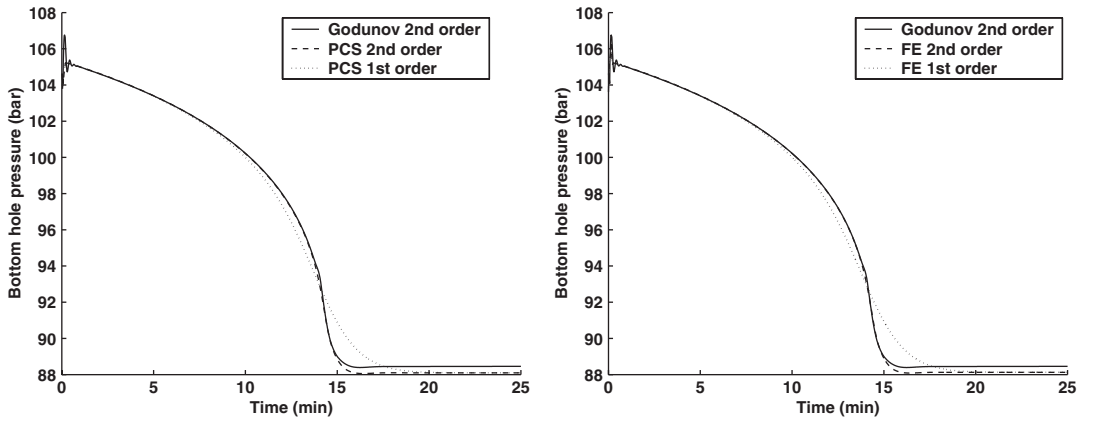

Figure 2. Bottom hole pressure as function of time in example 1.

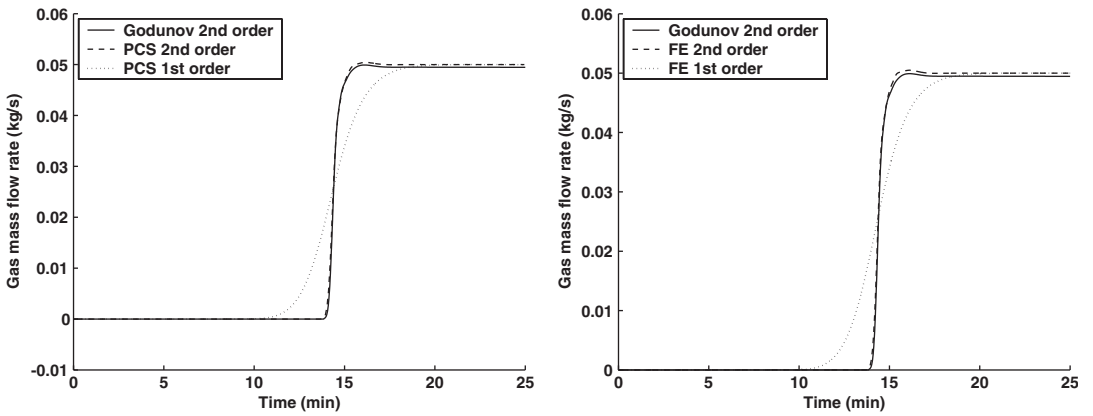

Figure 3. Outlet gas mass flow rate as function of time in example 1.

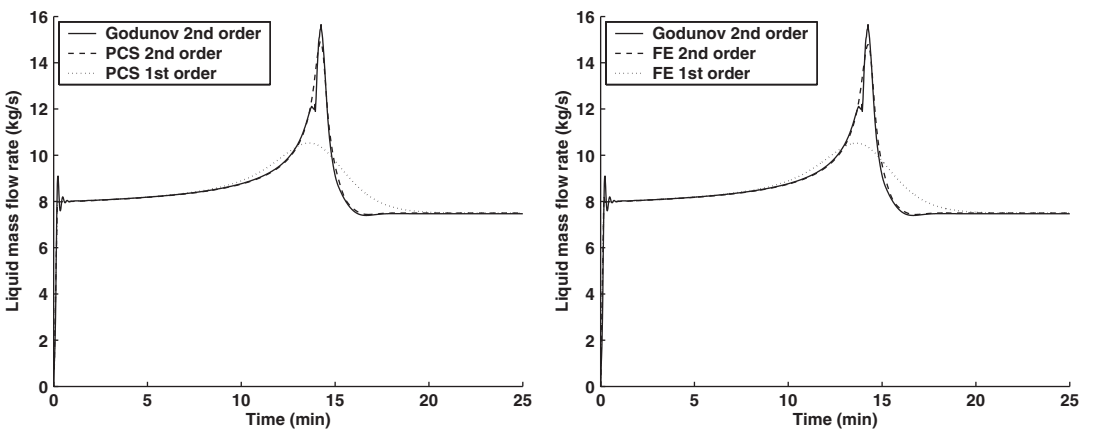

Figure 4. Outlet liquid mass flow rate as function of time in example 1.

when the different numerical schemes are used. Figure 5 shows the gas volume distribution at $t = 250,\ 500,\ 750$ and 1000 s.

The injection of gas in the drillstring causes the bottom hole pressure to decrease. The gas expands while it propagates towards the surface, and forces the liquid in front of the gas out of the well. Hence, a sharp peak in the outlet liquid rate is seen just prior to the gas is reaching the surface, see Figure 4. We observe that the second order schemes predict a quite sudden presence of gas at surface, see Figure 3. The first order schemes have problems with numerical diffusion which tend to smear out the sharp transition zone between the two phase mixtures and the liquid region in front of the migrating gas, see Figure 5. Hence, they will predict gas at surface at an earlier time, and the final steady state rates will be reached later. We also observe that the second order schemes are able to reconstruct the sharp peak in the liquid rate, while the first order schemes predict a much lower maximum value of this peak. This example shows that the second order version of the predictor corrector scheme and the FE approach give results that are quite comparable with the second order version of the Godunov scheme. Implementing slope limiter techniques in these simpler schemes, seems to have a very positive effect on reducing numerical diffusion related to mass transport. There is a small difference in the estimated steady-state bottom hole pressure, which is due to the different approaches used to treat the numerical boundary conditions. The numerical differences are however relatively small when compared to model error in the closure relations, see e.g. Reference [34].

In order to illustrate the relationship between the number of cells and the numerical diffusion, we show the predicted mass flow rates at the outlet when the spatial grid length is reduced from 20 to 2 m. The simulation is done using the first and second order finite element scheme. Figure 6 shows the simulated outlet rates of gas and liquid. The figure present the difference in the predicted results when using a first order scheme versus a second order scheme when using a grid length of 20 m. It also shows that maximum peaks in the flow rates are predicted to be even higher if we reduce the cell length from 20 to 2 m (using the

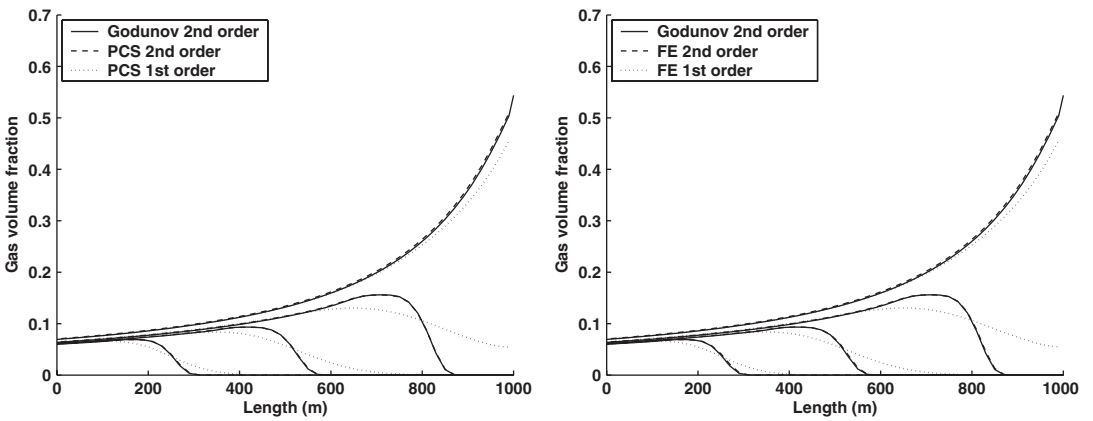

Figure 5. Gas volume fraction in example 1. The figures shows the distribution of gas in the well at times $t = 250,\ 500,\ 750$ and 1000 s. The first order scheme smears out the gas distribution.

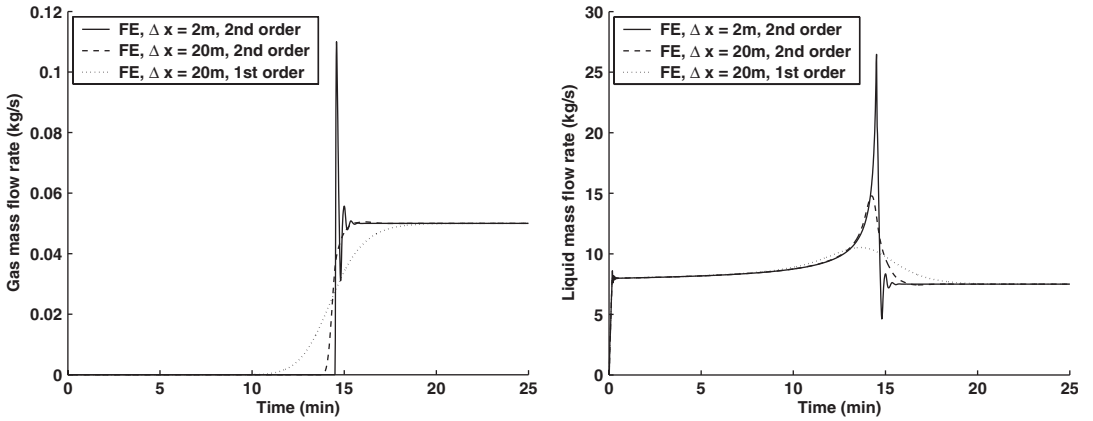

Figure 6. Outlet gas rate (left) and liquid rate (right) versus time in example 1.

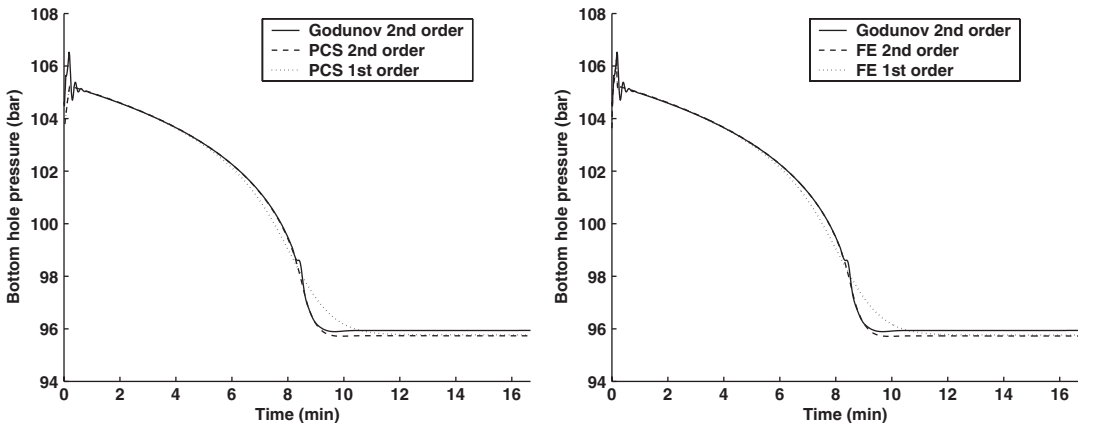

Figure 7. Bottom hole pressure as function of time in example 2.

second order FE scheme). This case also shows the importance of choosing a proper discretization with respect to the accuracy required. A smaller grid will increase the accuracy of the results. We observe that for the fine grid calculations, some oscillations can be observed. These oscillations occurring at approximately 15 min are a consequence of the dynamics generated by the sudden rate variations at the outlet. We note that more non-diffusive fronts can also be obtained by choosing a less diffusive slope limiter, e.g. SUPERBEE.

4.2. Example 2

This example is identical to example 1, except that the slip parameters $C_0 = 1.2$ and $C_1 = 0.55$ are used. These parameter values are approximations of the parameters used to calculate the gas velocity in slug flow. Figures 7–9 show the bottom hole pressure and the outlet flow rates. Figure 10 shows the gas volume fraction at $t = 250$, 500 and 750 s. We see that the gas phase

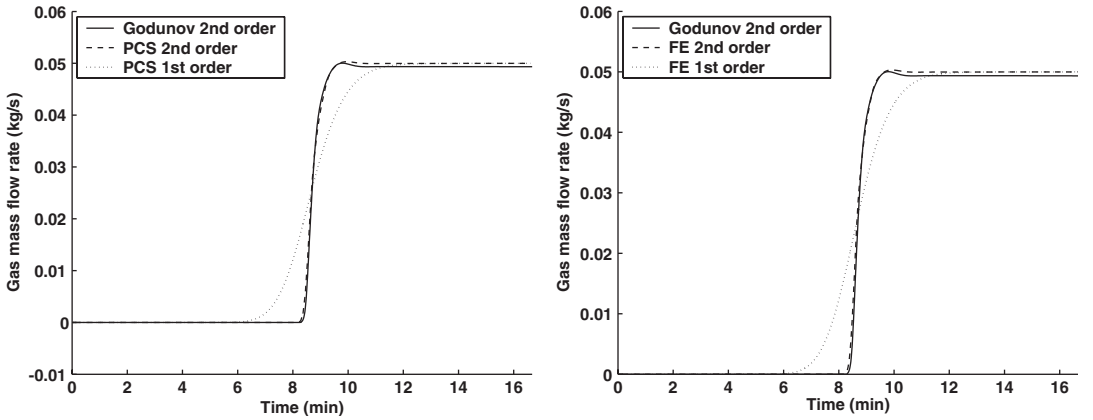

Figure 8. Outlet gas mass flow rate as function of time in example 2.

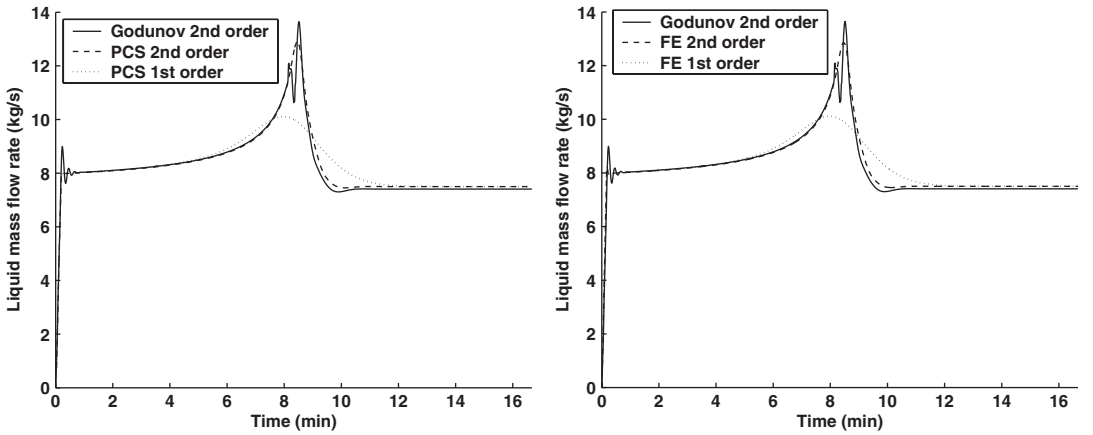

Figure 9. Outlet liquid mass flow rate as function of time in example 2.

is moving with a higher speed compared to example 1. The results are again satisfactory as the predictor–corrector shooting technique and the finite element approach are able to reconstruct the results obtained by the Godunov-type scheme. The irregularity in the liquid mass flow rate in the Godunov scheme, see Figure 9, is due to numerical inaccuracies related to the transition between two- and one-phase flow. The increased liquid velocity is amplifying this problem when compared to example 1.

4.3. Example 3

As a final example, we wish to investigate the ability to simulate a complex scenario caused by a shut down of the pumps. This leads to a situation where the injected gas migrates towards the surface, and liquid is forced in the downward direction (countercurrent flow). We use the same values for the slip parameters as in the previous example.

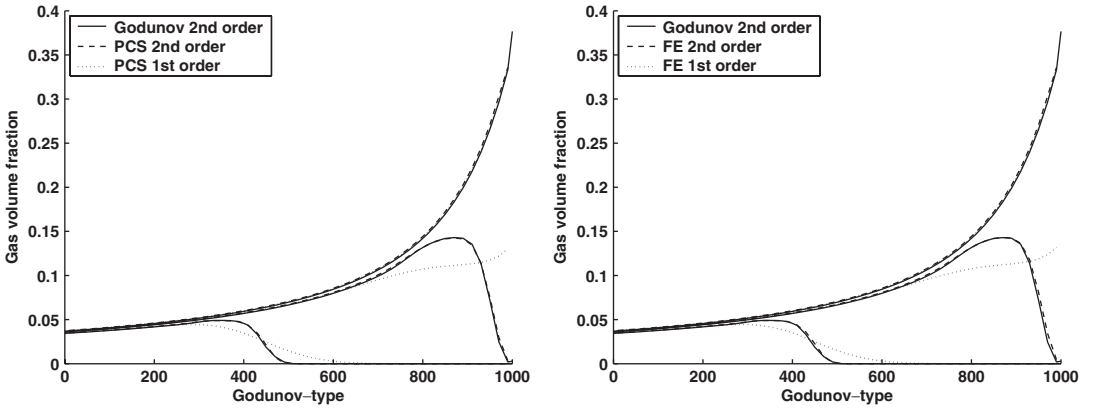

Figure 10. Gas volume fraction in example 2. The curves represent $t = 250$, 500 and 750 s.

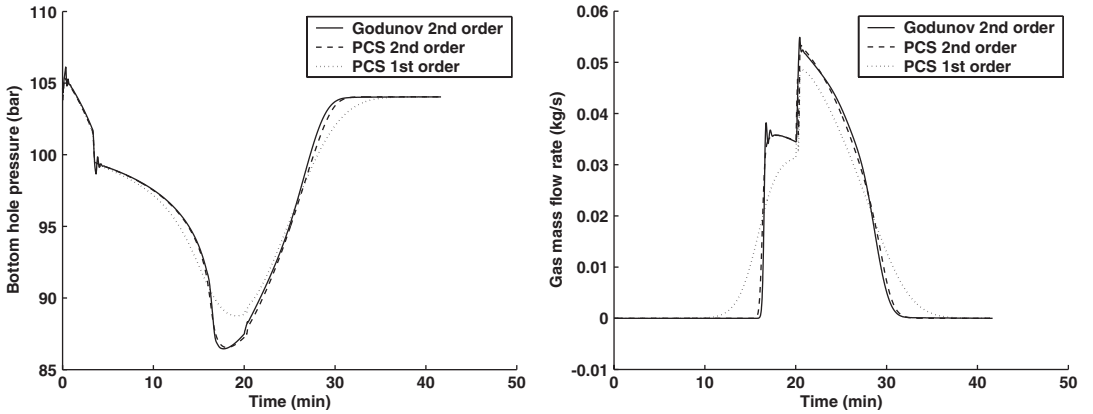

Figure 11. Bottom hole pressure and gas mass flow rate at the outlet as function of time in example 3.

The well is initially filled with stagnant liquid. The injection rates are then increased to 7.5 kg/s for liquid and 0.15 kg/s for gas during a 10 s period. The injection rates are kept constant in 200 s before the injection stops. The liquid rate at the outlet is now dropping to a value close to zero, see Figure 12. This leads to reduced wall friction which gives a sudden reduction in the bottom hole pressure at this time, see Figure 11. The sudden variations of mass flow rates at start-up and shut-down generate pressure pulses which are responsible for temporary oscillations of the flow variables. However, the oscillations are quickly damped by the frictional forces, and the amplitude is relatively small, see Figure 12 (right). The pressure pulses play therefore a minor role in these examples, and use of the no pressure wave model will not lead to large errors in e.g. an underbalanced drilling situation.

The injected mass flow rates are shut down in 1000 s, and during this period gas expands and migrates towards the surface. This gives a decrease of the bottom hole pressure, while the liquid mass flow rate in front of the gas increases. The gas reaches the outlet at approximately

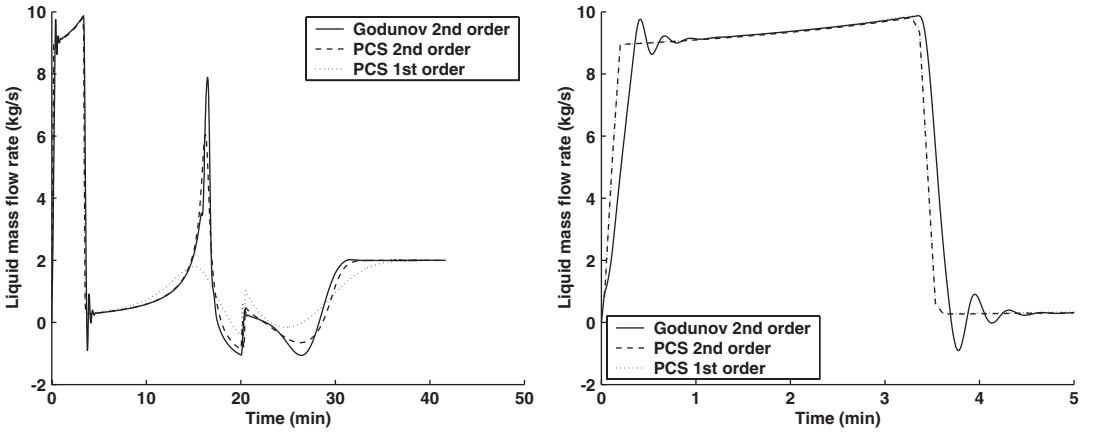

Figure 12. Outlet liquid mass flow rate as function of time in example 3. The right plot shows oscillations occurring in the vicinity of sharp gradients.

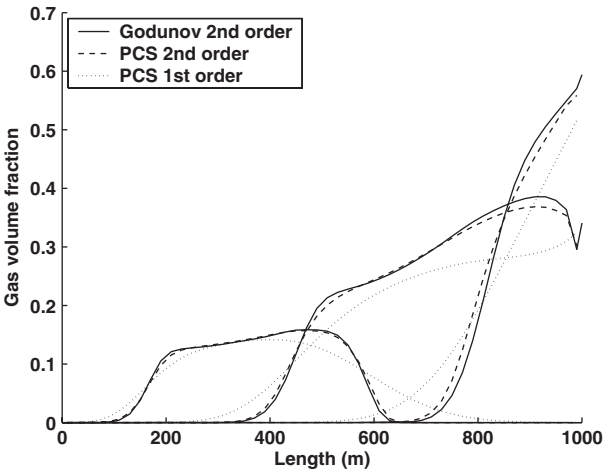

Figure 13. Gas volume fraction in example 3. The curves represent $t = 500$, 1000 and 1500 s.

17 min, and the expansion of gas is now forcing the liquid in a downward direction. The injection of liquid is resumed after 1200 s, and the rate is increased to 2 kg/s. The gas is now transported out of the well, and the hydrostatic pressure increases. Figure 13 shows the gas volume distribution at $t = 500$, 1000 and 1500 s.

5. CONCLUSIONS

The focus of this paper has been to show how traditional and simple numerical methods for simulation of multiphase hydrocarbon flow in pipelines, can be extended to second order

spatial accuracy. We have given an outline of modelling of one-dimensional two-phase flow in pipelines and wells, with emphasize on the drift flux model and the no pressure wave model. In addition, we have presented the basic solution strategies for the numerical methods discussed herein.

There is a need for accurate and reliable tools for prediction of hydrocarbon flow in pipelines and wells. We have shown how the non-diffusive MUSCL technique, originally developed to achieve higher order of accuracy in Godunov's method, can be integrated in simple semi-implicit schemes following the finite element technique and predictor–corrector shooting technique. These methods do not require numerical calculation of the Jacobi matrix and the corresponding eigenvalues and eigenvectors, and complex boundary treatment is not necessary. The MUSCL technique gives an overall reduction of the numerical diffusion, and complicated front tracking remedies are avoided.

We have made a rough estimate of the computational cost needed by the different numerical approaches, and conclude that the finite element approach has lowest cpu consume. The predictor–corrector shooting technique is somewhat slower due to the time consuming iterations needed on a local (within each box) and global (in order to match the outlet pressure) level. The traditional Godunov scheme suffers from time consuming numerical calculations of the Jacobi matrix, and can therefore not match either the finite element approach or the predictor–corrector shooting technique. These considerations substantiate the benefits of incorporating the MUSCL technique in more simple/traditional schemes.

From a modelling point of view, we have shown that the simplifications introduced by the no pressure wave model are of minor importance when the transients of interest are related to transport of mass (e.g. underbalanced drilling operations). The oscillations introduced by the pressure pulses have a small amplitude, and are only present in short periods following sudden rate variations.

We have presented several relevant examples where the Godunov-type method is compared with first and second order versions of the finite element method and the predictor–corrector shooting technique. The results show that numerical diffusion is reduced, and the second order versions of the schemes produce almost identical results.

APPENDIX

In this appendix we show some of the details in the flux functions written in terms of conservative variables. As shown in Section 2.2, the governing equations for two-phase flow can be written as a system of conservation laws

$$\frac{\partial \mathbf{u}}{\partial t} + \frac{\partial \mathbf{f}}{\partial x} = \mathbf{q}$$

The flux functions in terms of conservative variables can be written

$$f_1 = \frac{(1 - C_0)\rho_l u_3 + C_0 u_1 u_3 - C_1 \rho_l u_2}{(1 - C_0)\rho_l + C_0 u_1 + C_0 u_2}$$

$$f_2 = \frac{u_2(C_1 \rho_l + C_0 u_3)}{(1 - C_0)\rho_l + C_0 u_1 + C_0 u_2}$$

$$f_3 = \frac{u_2(C_1\rho_l + C_0u_3)^2}{((1-C_0)\rho_l + C_0u_1 + C_0u_2)^2} + \frac{u_1((1-C_0)\rho_l u_3 + C_0u_1u_3 - C_1\rho_l u_2)^2}{((1-C_0)\rho_l u_1 + C_0u_1^2 + C_0u_2u_1)^2} + \frac{\rho_1 a_g^2 u_2}{\rho_l - u_1}$$

The flux functions and the corresponding Jacobi matrix $\mathbf{A}(\mathbf{u})$ are very complex, and we have not found it reasonable to go into more details. In fact, in order to calculate the eigenvalues of $\mathbf{A}(\mathbf{u})$, it is necessary to express the hyperbolic system in terms of primitive variables

$$\mathbf{A}\frac{\partial \mathbf{V}}{\partial t} + \mathbf{B}\frac{\partial \mathbf{V}}{\partial x} = \mathbf{C}$$

where $\mathbf{V}$ is a vector containing physical variables. The eigenvalues then satisfies the following equation

$$det(\mathbf{B} - \lambda\mathbf{A}) = \mathbf{0}$$

Due to long calculations, this analysis is not included here, but more details can be found in References [24, 25]. The closure laws that have been used in this paper are very simple compared to what is used in practice. Both the slip relation and the density models are usually much more complex. This would complicate the analysis even more.

ACKNOWLEDGEMENTS

We thank the Norwegian Research Council for financial support through the Strategic Institute Program 'Complex Wells'. We also thank our colleagues Ove Sævareid and Erlend H. Vefring for useful discussions.

REFERENCES

1. TRAC-PF1/MOD1. An advanced best-estimate computer program for pressurized water reactor thermal-hydraulic analysis. *NUREG/CR-3858*, *LA-10157-MS*, Los Alamos National Laboratory, 1986.
2. Ransom VH *et al*. RELAP5/MOD1 Code Manual Volume 1: code structure, system models, and numerical method. *NUREG/CR-1826*, U.S. Nuclear Regulatory Commission, 1982.
3. Barre F *et al*. The CATHARE code strategy and assessment. *Nuclear Engineering Design* 1990; **124**:257–284.
4. Bendiksen K, Malnes D, Moe R, Nuland S. The dynamic two-fluid model OLGA: theory and application. *SPE Production Engineering*, May 1991.
5. Black PS, Daniels LC, Hoyle NC, Jepson WP. Studying transient multiphase flow using the pipeline analysis code (plac). *Journal of Energy Resources Technology* 1990; **112**:25–29.
6. Pauchon C, Dhulesia H, Lopez G, Fabre J. TACITE: a comprehensive mechanistic model for two-phase flow. *Proceedings of the Sixth International Conference on Multiphase Production*, Cannes, France, June 1993.
7. Pauchon CL, Dhulesia H, Binh-Cirlot G, Fabre J. Tacite: a transient tool for multiphase pipeline and well simulation. *The 1994 SPE Annual and Technical Conference and Exhibition*, New Orleans, LA, September 1994, SPE 28545.
8. Henriot V, Pauchon C, Duchet-Suchaux P, Leibovici CF. TACITE: contribution of fluid composition tracking on transient multiphase flow simulation. *Paper OTC 8563 Presented at the 1997 Offshore Technology Conference*, Houston, TX, 5–6 May 1997.
9. Faille I, Heintzé E. A rough finite volume scheme for modeling two-phase flow in a pipeline. *Computers and Fluids* 1999; 213–241.
10. Masella JM, Tran QH, Ferre D, Pauchon C. Transient simulation of two-phase flows in pipes. *International Journal of Multiphase Flow* 1998; **24**:739–755.
11. Ekrann S, Rommetveit R. A simulator for gas kicks in oil-based drilling muds. *Paper SPE 14182 Presented at the 1985 SPE Annual Technical Conference and Exhibition*, Las Vegas, 22–25 September 1985.
12. Nickens HV. A dynamic computer model of a kicking well. *Paper SPE 14183 First Presented at the 1985 SPE Annual Technical Conference and Exhibition*, Las Vegas, 22–25 September 1985.
13. White DB, Walton IC. A computer model for kicks in water and oil based muds. *Paper SPE 19975 Presented at the 1990 IADC-SPE Drilling Conference*, Houston, TX, 27 February–2 March 1990.

14. Bennion B. Evaluating reservoir performance improvements from underbalanced drilling operations. *Presented at the IADC Underbalanced Technology Conference and Exhibition*, Aberdeen, 27–28 November 2001.
15. Rolv Rommetveit, Vefring EH, Zhihua Wang, Taco Bieseman, Faure AM. A dynamic model for underbalanced drilling with coiled tubing. *Presented at the SPE/IADC Drilling Conference*, Amsterdam, 28 February–2 March 1995.
16. Fjelde KK. Numerical schemes for complex nonlinear hyperbolic systems of equations. *Ph.D. Thesis*, Department of Mathematics, University of Bergen, 2000.
17. Fjelde KK, Karlsen KH. High-resolution hybrid primitive-conservative upwind schemes for the drift flux model. *Computers and Fluids* 2002; **31**:335–367.
18. Frøyen J, Sævareid O, Vefring EH. Discretization, implementation and testing of a semi-implicit method. *Technical Report*, RF-Rogaland Research, 2000, Confidential.
19. Ishii M. *Thermo-Fluid Dynamic Theory of Two-Phase Flow*. Eyrolles: Paris, 1975.
20. Govier, Aziz. *The Flow of Complex Mixtures in Pipes*. Van Nostrand Reinhold: New York, 1972.
21. Coquel F, ElAmine K, Godlewski E, Perthame B, Rascle P. A numerical method using upwind schemes for the resolution of two-phase flows. *Journal of Computational Physics* 1997; **136**(2):272–288.
22. Tiselj I, Petelin S. Modelling of two-phase flow with second-order accurate scheme. *Journal of Computational Physics* 1997; **136**:503–521.
23. Toumi I, Kumbaro A. An approximate linearized Riemann solver for a two-fluid model. *Journal of Computational Physics* 1996; **124**:286–300.
24. Théron B. Ecoulements diphasique instationnaires en conduite horizontale. *Thèse*, INP Toulouse, France, 1989.
25. Benzoni Gavage S. Analyse numérique des modèles hydrodynamiques d'écoulements diphasiques instationnaires dans les réseaux de production pétrolière. *Thèse*, ENS Lyon, France, 1991.
26. Roe PL. Approximate Riemann solvers, parameter vectors and difference schemes. *Journal of Computational Physics* 1981; **43**:357–372.
27. Romate JE. An approximate Riemann solver for a two-phase flow model with numerically given slip relation. *Journal of Computational Physics* 1998; **27**(4):455–477.
28. Toro EF. *Riemann Solvers and Numerical Methods for Fluid Dynamics* (2nd edn). Springer: Berlin, 1999.
29. Hirsch C. *Numerical Computation of Internal and External Flows* (2nd edn), vol. 2. Wiley: New York, 1995.
30. LeVeque RJ. *Numerical Methods for Conservation Laws* (2nd edn). Birkhäuser: Basel, 1992.
31. Buffard T, Gallouet T, Herard JM. A sequel to a rough Godunov scheme: application to real gases. *Computers and Fluids* 2000; **29**:813–847.
32. Bram van Leer. Towards the ultimate conservative difference scheme. V. A second-order sequel to Godunov's method. *Journal of Computational Physics* 1979; **32**(1):101–136.
33. Bram van Leer. On the relation between the upwind-differencing schemes of Godunov, Engquist-Osher and Roe. *SIAM Journal on Scientific and Statistical Computing* 1984; **5**(1):1–20.
34. Lage ACVM. Two-phase flow models and experiments for low-head and underbalanced drilling. *Ph.D. Thesis*, Stavanger University College, Norway, 2000.

